FISEVIER

Contents lists available at ScienceDirect

Journal of the Mechanical Behavior of Biomedical Materials

dournal of the Mechanical Behavior of Bornedical Materials

journal homepage: www.elsevier.com/locate/jmbbm

Quantification of intracellular mechanical fields in invasive cancer cells using digital volume correlation, confocal microscopy, and finite element method

Aurélie Gangneux^a, Aymerick Gaboriau^b, Laetitia Caille^a, Marc Mesnil^b, Prasanth Bokam^c, Tanguy Vendeuvre^{a,d}, Stéphane Sebille^e, Norah Defamie^b, Arnaud Germaneau^{a,*}

- ^a Institut PPrime UPR 3346 CNRS Université de Poitiers ISAE ENSMA, France
- ^b CoMeT Laboratory, UR 24344 Université de Poitiers, France
- ^c Ansys France, Villeurbanne, France
- ^d Department of Orthopedic Surgery and Traumatology, University Hospital of Poitiers, France
- ^e PRéTI Laboratory, UR 24184 Université de Poitiers, France

ABSTRACT

Cell invasion process, which appears in the progression of tumours, such as glioblastoma, is highly dependent on cellular mobility. Cellular movement results from the interaction of chemical, biological and mechanical factors both inside and outside the invasive cancer cell. To identify and understand the relationship between these factors, it is necessary to quantify and visualise the extra- and intracellular kinematic fields during cell movement. This study proposes a new methodology for the experimental measurement of full kinematic fields inside cancer cells and the use of a digital twin simulation of the cell to obtain the stress and force fields. Confocal microscopy, Digital Volume Correlation (DVC) and Finite Element Method (FEM) are used in this methodology. To demonstrate the efficiency of this approach, highly invasive glioblastoma cells have been used as a model.

1. Introduction

Glioblastoma (GBM) is a malignant tumour of the central nervous system that is characterised by its aggressiveness and rapid growth (Louis et al., 2021). GBM remains incurable primarily due to its tendency to recur, driven by the capacity of tumor cells to infiltrate the adjacent healthy brain parenchyma beyond the boundaries of the resectable tumor mass (Ou et al., 2020). These invasive cells are characterised by their ability to form invadopodia, protrusions that extend from the cell into the extracellular matrix (ECM) (Wolf et al., 2007; Chepied et al., 2020). Invadopodia facilitate degradation of the ECM, promoting invasion of healthy tissue. The kinetics of invadopodia formation is influenced by the stiffness and density of the ECM, which can enhance matrix degradation (Parekh et al., 2011; Masi et al., 2020). Consequently, invadopodia exert protrusive forces that depend on the physical characteristics of the ECM. Understanding these physical interactions requires quantitative approaches capable of visualising and measuring intracellular stresses and force fields.

Analysis of cellular motility is crucial to a wide range of physiological and pathological processes, including wound healing, inflammatory responses, bone regeneration, and cancer cell migration. Over the past

few years, several techniques have been developed to quantify cell kinematic and understand their underlying mechanisms.

Particle Tracking (PT) was one of the first methods developed to quantify the displacement of cells by linking them to a point (Dembo and Harris, 1981; Qian et al., 1991; Saxton and Jacobson, 1997). In this method, cells are marked with contrast agents or fluorescent markers. The 2D or 3D images of the cell's temporal evolution are acquired using microscopes adapted to the size and type of marker chosen. Segmentation algorithms are then employed to identify the cells in each image. The position of the cell's centroid is computed for each segmented image and connected using techniques such as mean square displacement to obtain the trajectory of each cell (Manzo and Garcia-Parajo, 2015; Meijering et al., 2012). Although PT provides insight into morphology, trajectories and velocities, its discrete nature means that each marker yields only a single measurement point, limiting access to continuous mechanical fields (Emami et al., 2021; Pushkarsky et al., 2014). Extensions of PT have been developed to track smaller particles and molecules, both inside and outside cells (Chenouard et al., 2014; Sergé et al., 2008; Wang et al., 2021; Weihs et al., 2006), thereby enhancing our understanding of intracellular processes and exchanges, but these approaches remain constrained by the same discretization limitation.

E-mail address: arnaud.germaneau@univ-poitiers.fr (A. Germaneau).

^{*} Corresponding author.

Other techniques, such as Traction Force Microscopy (TFM), quantify mechanical fields at the cell-substrate interface (Dembo and Wang, 1999; Lekka et al., 2021; Sabass et al., 2008). In TFM, fluorescently labelled cells adhere to a substrate embedded with fluorescent beads, whose displacements are tracked using PT, Particle Image Velocimetry (PIV), Particle Tracking Velocimetry (PTV) (Sanz-Herrera et al., 2021; Trepat et al., 2009), or Digital Image Correlation (DIC) and Digital Volume Correlation (DVC) (Holenstein et al., 2019; Mulligan et al., 2018; Toyjanova et al., 2014). From these bead displacements, stress and force fields within the substrate are reconstructed by the finite element method (FEM). TFM has been successfully implemented in both 2D (Butler et al., 2002; Schwarz and Soiné, 2015) and 3D by embedding the cell in a substrate (Apolinar-Fernández et al., 2023; Legant et al., 2010), and remains a reference to investigate cell-substrate interactions. However, it only accesses forces transmitted through the substrate, without revealing the full-field intracellular mechanics driving invadopodia formation.

Beyond substrate-based methods, atomic force microscopy (AFM) has enabled precise mechanical characterization of living cells, including system identification of viscoelastic properties (Rico et al., 2005), advanced modelling of large-deformation indentation (Shen et al., 2020), and system identification approaches for extracting viscoelastic parameters from AFM indentation curves (Bahwini et al., 2022). AFM has also been applied to quantify the mechanics of brain cells (Bahwini et al., 2018), providing key insights into cell-specific mechanics in the central nervous system.

At the molecular scale, computational studies have further highlighted the role of mechanics in biological regulation. Khataee et al. (2018) showed that assisting forces accelerate kinesin unbinding from microtubules, illustrating the force-dependence of molecular interactions. In a previous work, Khataee et al. (2013) demonstrated how computational nanotechnology can predict structural and physical indices of the smallest fullerene (C20), highlighting the power of graph-based modeling for nanoscale systems. These studies emphasize the importance of multiscale approaches, from molecules to cells, to capture the full complexity of mechanobiology.

Taken together, these approaches underline the lack of methods capable of providing volumetric, full-field intracellular mechanics. Our hypothesis is that coupling Digital Volume Correlation (DVC) with finite element modelling enables robust estimation of intracellular stress and force distributions. The motivation of this work is to overcome the limitations of existing methods that focus either on substrate mechanics or point measurements by providing a full-field description of intracellular mechanics. By extending computational paradigms demonstrated at the nanoscale (Khataee et al., 2013; Khataee et al., 2018) and at the single-cell level (Bahwini et al., 2018, 2022; Shen et al., 2020) to the scale of whole living cells, our work introduces an integrated framework bridging imaging, computation, and mechanobiology. This approach has significance for cancer research, as it allows quantifying how invasive glioblastoma cells generate and transmit forces during invadopodia formation, a process central to their invasive potential.

Here, we present an innovative methodology combining Digital Volume Correlation, high-resolution confocal microscopy, and FEM to provide a detailed quantification and visualization of intracellular displacement, stress, and force fields in invasive cancer cells.

2. Materials and methods

2.1. Cell culture and substrate preparation

The human glioblastoma cell line Ln229 was used in this study. Cells were cultured in DMEM (Dulbecco's Modified Eagle Medium) supplemented with 10 % fetal calf serum and 1 % antibiotics (penicillin and streptavidin) in a water-saturated incubator (37 $^{\circ}$ C, 5 % CO₂).

2.2. Fluorescent-gelatin degradation assay on insert and invadopodia observation by confocal microscopy

To assess the ability of cells to form invadopodia and to degrade matrix, the cells were plated on inserts (10⁴ cells/mL) coated with 0.2 % fluorescent Oregon Green® 488-conjugated gelatin (FG-gelatin; Molecular Probes, Eugene, USA), in 24-well plates and maintained in a watersaturated incubator (37 °C, 5 % CO₂) during 8 h. To do so, inserts were prepared as follows. 50 μL of 0.2 % FG-gelatin were added on 1 μm diameter pored inserts. 30 μL of FG-gelatin were then removed and inserts were incubated at room temperature for 1 h, before putting them at 37 °C for 2 days/2 nights. Once the cells were seeded, indirect immunofluorescence was performed at different times. The immunodetection of actin in the Ln229 cells seeded on the inserts coated with FG-gelatin was performed by using a mouse antibody (Sigma-Aldrich). The cells were fixed in paraformaldehyde (4 %) for 20 min at room temperature. After incubation in a blocking solution (2 % bovine serum albumin, 1 % Triton X-100 in PBS), the cells were incubated with primary antibodies (anti-actin 1:250) overnight at 4 °C. Mouse Alexa Fluor® 555- conjugated secondary antibodies (1:250, Invitrogen) were then applied to the preparations for 1 h. Coverslips or inserts were mounted afterwards with Mowiol (Calbiochem, Darmstadt, Germany) prior to observation with confocal microscopy.

In our confocal microscopy setup, fluorescent signals were acquired in the green channel (488 nm) and the red channel (545 nm). In a first step, invadopodia activity was assessed by detecting dark areas corresponding to degraded regions of the FG-gelatin (488 nm). In a second step, the presence of invadopodia was confirmed in these degraded areas by co-localization with actin, detected in the red channel (545 nm). Confocal images were obtained using an Olympus IX81 laser scanning confocal inverted microscope with 40X (UAPO ID/340UV NA 135) or 60X (O.N. 1.4 PLAPO) oil objectives. Images were processed with FluoView software. Imaris software was used for the 3D reconstruction.

In addition, a Boyden chamber device was used to confirm invado-podia formation. This device allows Ln229 cells to be seeded on a filter previously coated with fluorescent gelatin. The filter contains 1- μm diameter pores, which permit only the invadopodia to extend into the lower chamber while preventing passage of the entire cell. After actin immunofluorescence staining, invadopodia could be visualized in 3D reconstructions at the level of these pores.

2.3. Volume images acquisition by confocal microscopy

Cultured Ln229 cells were labelled with fluorochromes at the plasma membrane (DiD, red emission) and at the actin cytoskeleton (RFP, red emission). This labeling was chosen to enable visualization of the entire cell on confocal microscopy images. They were seeded on a green fluorescent gelatin substrate (Oregon Green 488 conjugated®Gelatin), which was coated on glass coverslips. The cells adhered to the substrate after incubation for 2 h at 37 °C. Imaging of cells and substrate was performed using an Olympus FV3000 confocal 'rotating disc' microscope (Revolution/Andor) equipped with a 60X UPLSAPO NA 1.35 oil objective. To excite cells and substrate fluorescence, 560 nm and 488 nm laser wavelengths were respectively used. Volume images were acquired at a resolution of 512x512 pixels and 156 depth images were collected every 6 min for a total of 20 h. Voxel size was 0.29 x 0.29 x 0.4 μm . Confocal imaging was conducted at 37 °C using an enclosure heated and regulated with 5 % CO₂. In this experiment, images of three cells were captured on the same substrate. The cells were selected based on their distance from other cells in the environment to limit the interaction between them.

2.4. Digital volume correlation

Displacement fields in the cells between two images were measured using Digital Volume Correlation (DVC, X-DVCorrel) (Germaneau et al.,

2007; Valle et al., 2019). This technique uses grey-level distributions of volume images to determine the material transformation between a reference volume and the deformed state volume of a cell. To compare images, a region of interest (ROI) was defined and divided into subsets, with a size of 32 x 32 x 32 voxels. A search zone was defined around each subset and degrees of similarity between the fixed initial subset and the deformed subset was computed at each position within this zone. The displacement between subsets was defined by the maximum similarity, and tricubic interpolation was used to achieve sub-voxel accuracy. Parameter tests were preliminarily conducted to determine optimal subset and search zone sizes.

Displacements were computed incrementally, i.e., each volumetric image stack was correlated with the immediately preceding one rather than with the first time point. This strategy minimized decorrelation effects due to large deformations or intensity changes and improved robustness for live-cell imaging.

To restrict the analysis to cell structures and reduce computation time, a binary mask of the cell was applied. This mask was generated by segmenting the reference volume using Python and the Skimage library. Segmentation involved denoising the volumetric images with a median filter followed by a watershed algorithm (Kornilov and Safonov, 2018). Importantly, this filtering was applied exclusively during the segmentation step to delineate the cellular region of interest. The DVC computations themselves were performed directly on the original confocal image stacks, without any filtering or preprocessing.

Noise quantification through a conventional zero-strain test was not feasible because live cultured cells exhibit intrinsic motion between acquisitions. Nevertheless, the measured displacements ($-2~\mu m$ to $+2~\mu m$) are well above typical noise levels reported in confocal DVC of hydrogels, which achieve sub-micron precision (Franck et al., 2007). This supports the robustness of the present measurements.

During DVC analysis, the substrate was treated as the stationary reference. Correlation was restricted to the segmented cellular volume, excluding the substrate. Therefore, non-zero displacements observed at the basal plane represent the relative motion of the cell base with respect to the fixed substrate. These basal displacements are biologically relevant, reflecting cell motility and mechanical interaction with the substrate. The strain field was then computed from the measured displacement field.

2.5. Numerical model

A finite element model was developed to determine stress distribution and the reaction forces exerted by the cell on the substrate. Cell geometries were extracted from segmented volumetric images. Each cell was imaged every 6 min over a period of 20 h, resulting in 200 geometries capturing the cell's evolution. Finite element simulations were conducted using ANSYS software (version 24.R1). The nodes at the cell boundaries were constrained with experimentally measured displacements obtained from DVC, while the remaining surfaces were considered free of constraints (stress-free boundary). A homogeneous, isotropic, linear elastic material model was adopted for the cell, with a Young's modulus of 0.5 kPa based on literature values (Pogoda et al., 2014). Although simplified, this provides a suitable first-order approximation. A mesh composed of voxel-sized hexahedra elements (0.29 x 0.29 x 0.4 μ m) was applied to each geometry, with an average cell consisting of 150.000 elements.

3. Results

3.1. Invadopodia formation

The human glioblastoma Ln229 cells have the ability to form invadopodia, which are necessary for their invasive process (Fig. 1). These membrane invadopodia, rich in actin fibers, have the ability to degrade gelatin and lengthen under the ventral face of the cells. Fig. 1 gives an

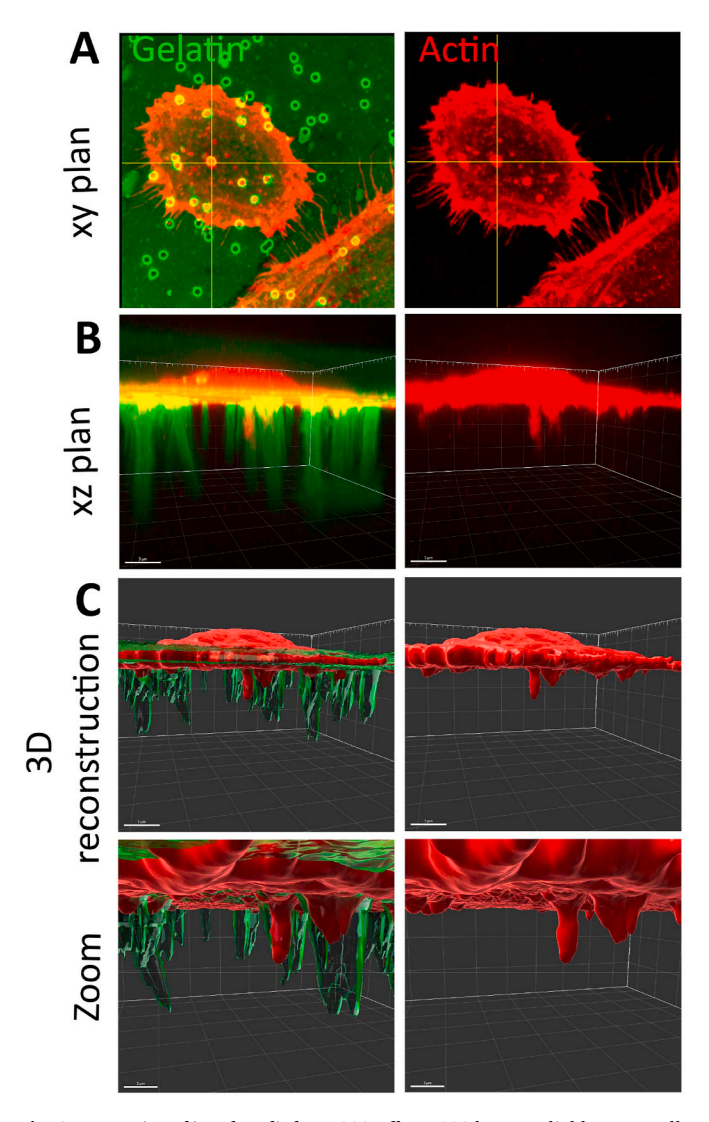


Fig. 1. Formation of invadopodia by Ln229 cells: Ln229 human glioblastoma cells were seeded on inserts (1 μ m-diameter pores) coated with green-Gelatin matrix. A) Confocal microscopy images of the Ln229 cells in xy plan (left panel: merge image with gelatin in green and actin in red; right panel: actin in red). B) Confocal microscopy images of the Ln229 cells in xz plan (left panel: merge image with gelatin in green and actin in red; right panel: actin in red) in Imaris software. C) First line of panels: Invadopodia were observed below the cells by 3D reconstruction (Scale bars: 5 μ m). Second line of panels: Different zoomed views of the labelled invadopodia.

example of 3D reconstruction of invadopodia after staining the actin fibers by immunofluorescence.

It should be noted that, while the confocal microscopy images in Fig. 1 specifically illustrate invadopodia formation in Ln229 cells, the subsequent mechanical analyses using Digital Volume Correlation (DVC) and Finite Element simulations, presented in Figs. 2–5, were performed during general cell motility conditions without specifically selecting periods or regions characterized by active invadopodia formation. The aim here was to quantify the general intracellular mechanical environment rather than exclusively analyzing mechanical fields associated directly with invadopodia.

3.2. Measuring displacement

In order to analyze the formation of invadopodia from a mechanical perspective, volumetric images of three cells were acquired over time using confocal microscopy. Representative displacement fields

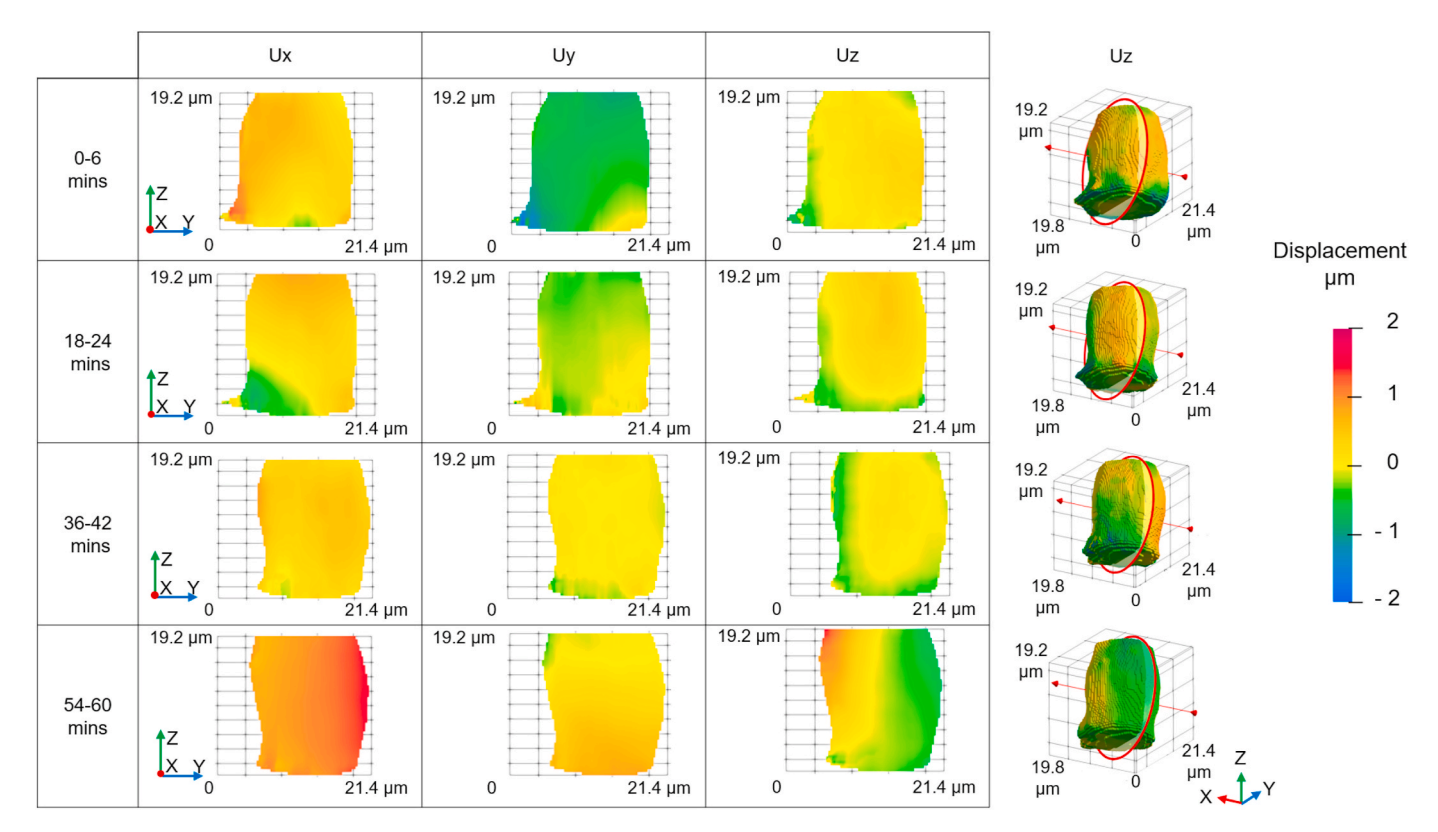


Fig. 2. Temporal evolution of intracellular displacement fields measured across the entire cell volume (including cytoplasm, nucleus, and invadopodia) over a 6 min interval. The left columns present cross-sectional views of the displacements Ux, Uy, and Uz, while the right column displays external 3D visualizations of the displacement Uz. The displacement values are scaled between $-2 \mu m$ and $+2 \mu m$.

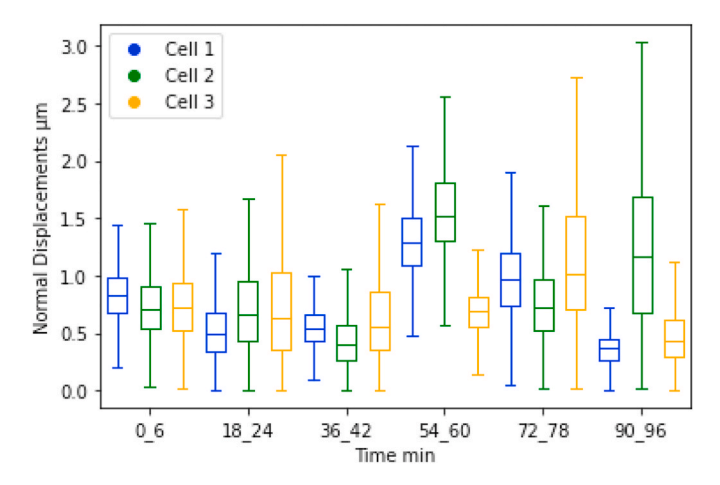


Fig. 3. Normal displacements measured for three cells adhered to the same substrate over a $2\ h$ period. Initially, all cells displayed similar amplitudes of normal displacements during the first 6 min. Each cell then exhibited its own characteristic behaviour, with periods of stability followed by displacement peaks.

measured in glioblastoma cells are shown in Fig. 2. These displacement fields represent global intracellular mechanical activity, including all cellular structures (e.g., cytoplasm, nucleus, invadopodia, and cell membrane), and are not specifically focused on isolated invadopodia structures. Movement within the cell was both continuous and homogeneous, with localised regions showing increased activity. Significant displacements were observed in all directions in the lower part of the cell, where there was contact with the substrate. Pronounced movements were also observed at periphery of the cell, often with opposing displacements between one side of the cell and the other. The central region, likely corresponding to the nucleus, displayed comparatively

small and uniform displacements close to 0 in all directions. For example, between 54 and 60 min, the displacements Uz of the cell along the y axis ranged from $2\,\mu m$ to ${-}1\mu m$. Looking at Ux, the entire cell moves by $1{-}2~\mu m$. The Uy followed a gradient with values close to zero at the top of the cell and reaching 1 μm at the bottom. This suggests that the cell moves positively along the XY direction, exhibiting an internal downward motion in the same direction, while an upward movement occurs in the opposite direction.

To study the evolution of global movement over time, three cells adhered to the same substrate were analyzed. Fig. 3 shows the normal displacement of these three cells over a 2 h period. During the first 6 min, all cells exhibited similar behaviour, with displacements ranging from 0 to 1.5 µm, and a median around 0.7 µm. After this initial phase, each cell exhibited distinct patterns. Cell 1 showed the smallest displacements with little variability. For instance, between 36 and 42 min and between 90 and 96 min, its displacements were within a range of 1 μ m, with quartiles around 0.3 μ m, indicating a stable movement. Cell 2 exhibited more varied displacements, with peaks reaching 3 µm, particularly between 90 and 96 min. Cell 3 also showed peak displacements between 18 and 24 min, then between 72 and 78 min, followed by more stable periods, with quartiles indicating displacements of around 0.5 µm. Despite similar initial displacement patterns and environmental conditions, each cell demonstrated unique displacement values and variations over time. Nonetheless, a common pattern emerged: displacement peaks were typically followed by phases of stabilization.

3.3. Cell simulation

The cell geometries over time were extracted using a segmentation algorithm and then meshed. At each node, the displacements measured by DVC were applied, and a Young's modulus of 0.5 kPa was uniformly applied across the cell. The finite element method (FEM) was used to compute the time evolution of the internal stress fields and reaction

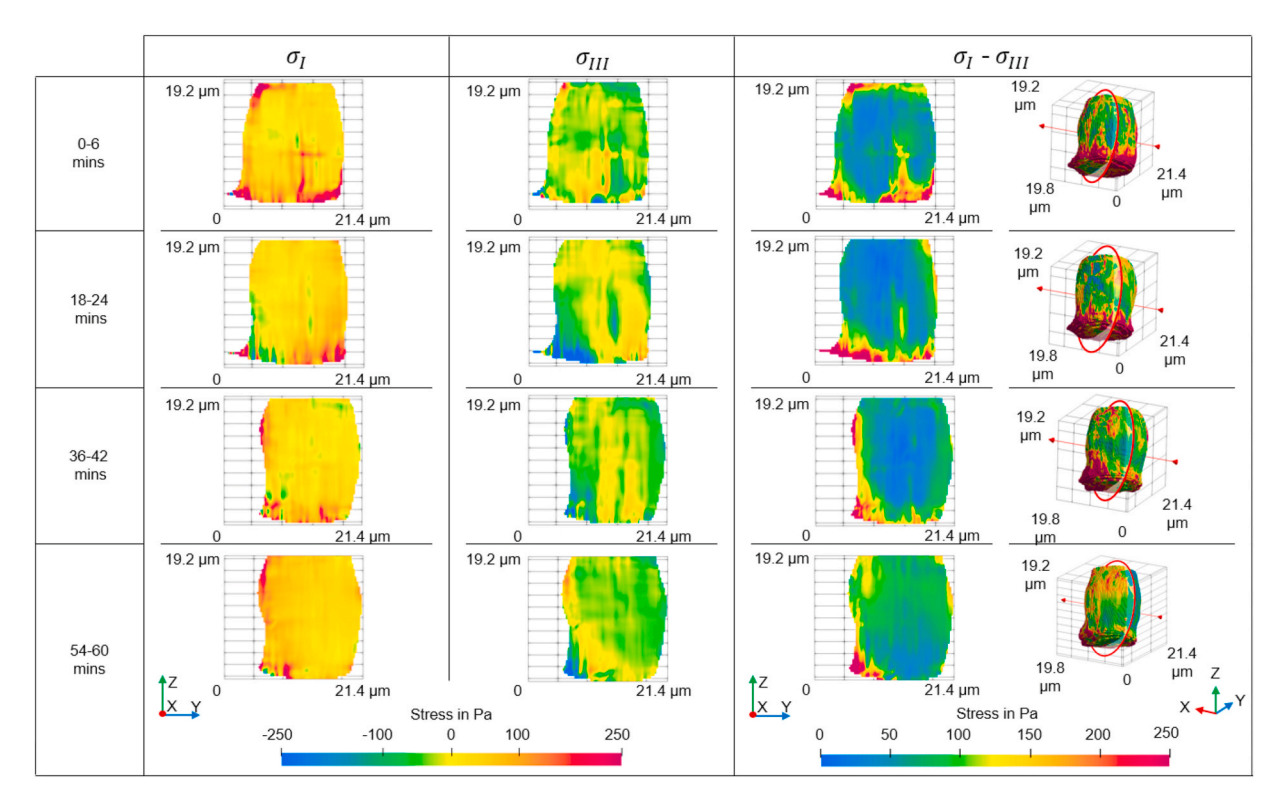


Fig. 4. Spatiotemporal evolution of principal stress fields inside a single cell over 1 h. Each row corresponds to a different time interval (0–6, 18–24, 36–42, and 54–60 min). The first three columns display 2D cross-sections through the 3D cell volume, showing the maximum principal stress σ_I (tension), the minimum principal stress σ_{III} (compression), and their difference $\sigma_I - \sigma_{III}$. The last column presents 3D renderings of $\sigma_I - \sigma_{III}$.

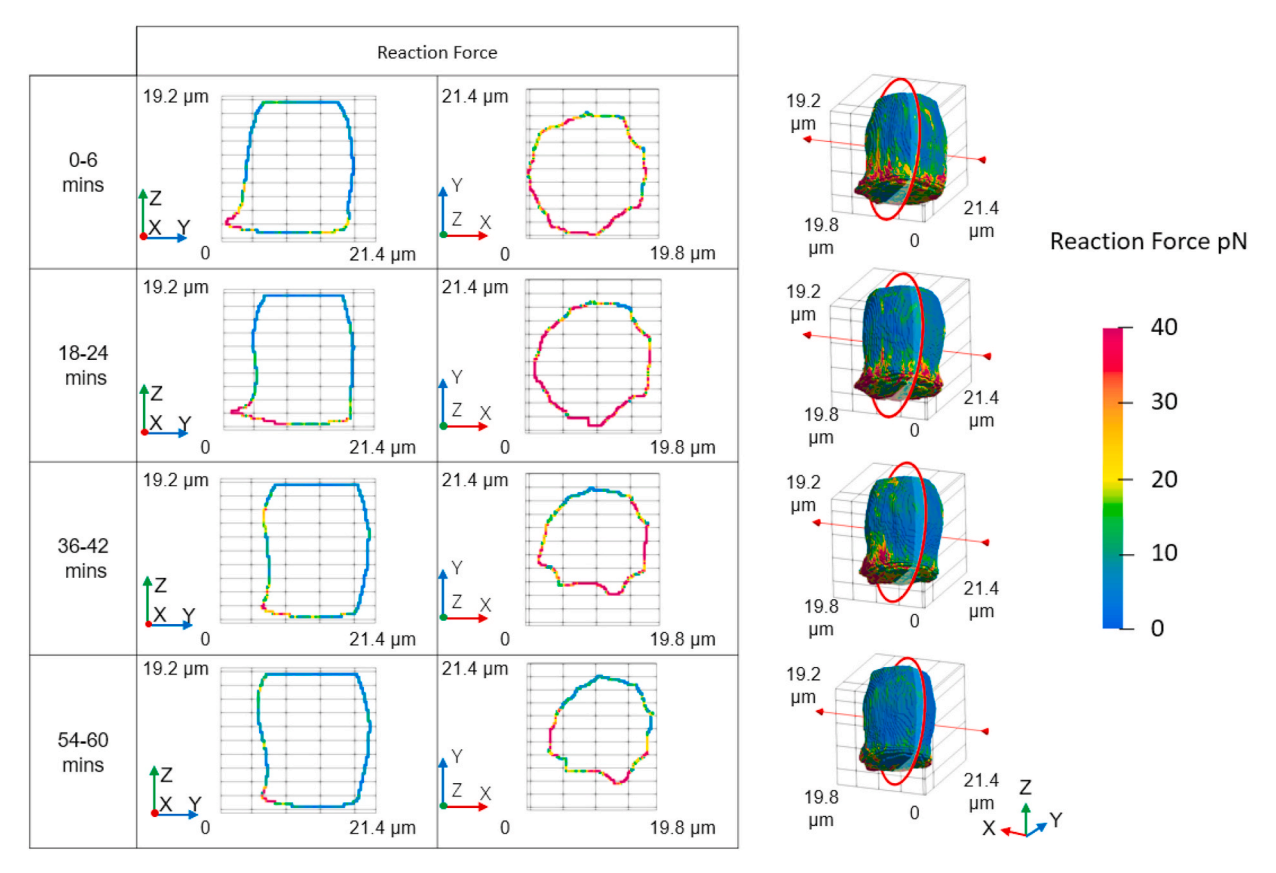


Fig. 5. Reaction force results for Cell 1 over a 1 h period. The 3D views on the right illustrate the spatial distribution of the reaction force (in pN) over time. The left columns show sectional views along the Y and X directions at four specific time intervals (0–6, 18–24, 36–42, and 54–60 min). The forces are scaled within a range from 0 pN to 40 pN.

forces in Cell 1. The principal stresses σ_I and σ_{III} (Fig. 4) range from 250 Pa to -250 Pa, indicating maximal and minimal stress, respectively. The results show that the cell is mostly in traction at all times, with an average internal value of 50 Pa. Over time, the cell's contours, particularly the upper and lower parts, were the most exposed to the highest traction forces. Locally, compression zones were observed at the center of the cell and partially along its contours. The difference between σ_I and σ_{III} indicates the presence of internal shear stresses reaching up to 250 kPa. These shear stresses were mainly concentrated in the lower part of the cell, in contact with the substrate, and occasionally extended from the cell boundary to the center.

The Finite Element Method (FEM) enables the calculation of the reaction forces at the cell's boundary. Fig. 5 shows the reaction force exerted by the cell on its environment, with a maximum value of 40 pN. The maximum force was concentrated at the interface between the lower region of the cell and the substrate. Additionally, this force wa directed opposite to the overall motion of the cell. This suggests that the strongest interactions occur at the cell-substrate interface, which plays a critical role in the dynamics of cell motility.

4. Discussion

This study presents a new approach for measuring displacement fields and computing stress and force distributions within cells. By combining confocal microscopy with volumetric image correlation and finite element analysis, this method provides a more comprehensive view of the mechanical environment inside the cell compared to traditional techniques. Unlike particle tracking or traction force microscopy, which mainly offer local or edge-specific data, our approach enables a more detailed mapping of the internal mechanical fields throughout the entire cell. Moreover, this method is non-invasive, as labelling process does not damage the cells, allowing for observation over extended periods of several hours. The ability to capture images at short intervals makes it particularly effective for monitoring fast, dynamic biological processes, such as invadopodia formation, thus opening new avenues for studying cellular behaviour in real time. The formation and development of invadopodia of glioblastoma cells is a relatively unexplored topic in the mechanical literature. In this study, the human glioblastoma Ln229 cells, which are able to form invadopodia, demonstrated normal displacements ranging from 0 to 3 μm over a 6 min period. The non-zero displacements measured at the basal plane do not indicate motion of the substrate, which was considered fixed, but instead correspond to the relative motion of the cell base with respect to the substrate. This motion is biologically meaningful, as it highlights the active displacement of the cell during invasion. These internal displacements were not uniform; higher values were observed in the lower part of the cell and in the X and Y directions, rather than in the Z direction. Consequently, cells deposited on the substrate tend to move predominantly within the plane of the substrate. The variability observed between cells in terms of displacement and stress distributions (Fig. 3) may reflect differences in invadopodia activity and cytoskeletal remodeling. Such heterogeneity is consistent with the notion that only a subset of glioblastoma cells display high invasive potential. Our methodology thus provides a means to capture biologically relevant mechanical diversity at the single-cell level. Literature indicates that cellular displacements are dependent on a variety of parameters, including environmental conditions, cell type, and the time interval between volumetric image acquisitions. For example, fibroblasts analyzed using 2D TFM exhibited displacements ranging from 0 to 1 µm over a 35 min period (Franck et al., 2011), while human airway smooth muscle (HASM) cells, stimulated with histamine, showed displacements up to 3 µm within 6 min (Butler et al., 2002). These observations suggest that the displacement values for Ln229 cells obtained through this novel approach are in line with literature for other cell types. Additionally, the concentration of displacements at the cell-substrate interface observed in this study is consistent with previous findings using 2D TFM for fibroblast cells (Doyle et al., 2022),

reinforcing the idea that cell adhesion to the substrate plays a crucial role in displacement dynamics.

Despite the innovative approach presented, we acknowledge important limitations. Direct validation of computed displacement and stress fields at the cell-substrate interface via established experimental techniques such as TFM was not performed. Additionally, assuming cellular mechanics as homogeneous and purely elastic neglects the known structural heterogeneity and viscoelastic behavior of cells. Similar simplifying assumptions have been used in advanced AFM-based studies, such as Shen et al. (2020) and Bahwini et al. (2022), where indentation models were applied to extract effective viscoelastic parameters of adherent cells. These works, along with earlier AFM studies of neuronal cells (Bahwini et al., 2018), show that reduced-order models, while not fully capturing heterogeneity, can still yield biologically meaningful insights. Future improvements of this method will include experimental validation via TFM and integration of more realistic viscoelastic mechanical models.

TFM remains the gold standard for quantifying forces at the cell-substrate interface. The displacement fields reconstructed in our study are consistent in magnitude with those reported in recent TFM studies. Monzo et al. (2021) observed substrate displacements of \sim 1-2 μm at the poles of invasive glioblastoma cells, while Cheung et al. (2025) reported matrix displacements of 1-5 µm in invasive breast cancer cells embedded in collagen-based matrices. These values are comparable to the intracellular displacements measured here (-2 to +2 μ m), supporting the biological plausibility of our results. Similarly, the reaction forces reconstructed in our study are in the same range as the forces reported in these TFM studies. Importantly, while TFM quantifies extracellular deformation and traction, our DVC-FEM framework provides volumetric maps of intracellular stress and strain fields. This constitutes the fundamental novelty of our approach, bridging extracellular force quantification with intracellular mechanobiology in the context of cancer cell invasion.

However, TFM is inherently limited to substrate deformation and does not provide direct access to intracellular mechanics. The approach introduced here is complementary, as it enables full-field quantification of intracellular stress and strain distributions. Although no direct validation against TFM was conducted in the present study, future work combining both methodologies will be essential to establish a comprehensive and validated framework for cell mechanobiology.

At the molecular and nanoscale, complementary studies have also shown how mechanics regulates biological function. Khataee et al. (2018) demonstrated that kinesin-microtubule unbinding is accelerated by assisting forces, while Khataee et al. (2013) highlighted the structural response of C20 fullerenes using computational nanomechanics. These examples illustrate that across scales, from molecules to whole cells, mechanical forces govern function and simplified models remain necessary for tractable analysis. Our study extends these principles by applying a volumetric, full-field approach at the cellular level, thereby bridging nanoscale mechanics with whole-cell mechanobiology.

The method introduced in this study also allows the extraction of cell geometries from confocal microscopy images. The shapes observed were predominantly spherical or oval with minimal spreading, consistent with previous studies for a substrate with a Young's modulus of 0.5 kPa (Pogoda et al., 2014). In order to compute the stress and force fields, a finite element model of the cell during invasion was created by meshing these geometries. Finite element models of cells and substrates with 2D and 3D TFM are described in the literature. In these models, boundary conditions are defined by the displacements measured within the substrate and the input mechanical behaviours are those of the substrate (Hur et al., 2009; Sanz-Herrera et al., 2021; Song et al., 2019). In contrast, the method proposed here uses the internal displacements of the cell, measured by DVC as boundary conditions and the model's material properties are those of the cell. Previously, it was shown that Ln229 cells exhibit linear behaviour with a Young's modulus of approximately 0.3 kPa (Pogoda et al., 2014). Our approach provides a

more comprehensive analysis by simulating not only the stresses at the cell boundary but also within the cell itself. The results from this study show that internal stresses range from 0 to 0.25 kPa when cells are placed on a substrate with a Young's modulus of 0.5 kPa. These values are consistent with existing literature, which reports similar stress amplitudes for various cell types and substrates. For example, 2D TFM has demonstrated that fibroblasts generate traction stresses ranging from 0 to 0.25 kPa over 6 h on a polyacrylamide substrate with a Young's modulus of 3 kPa (Yang et al., 2006). Similarly, human T24 bladder cancer cells exert traction stresses between 0.2 and 0.8 kPa every 2 min on polyacrylamide substrates with stiffness ranging from 2 to 10 kPa (Peschetola et al., 2013).

Another limitation arises from the 6-min acquisition required for a full 3D confocal stack. During this period, cells may continue to deform, so the displacement and strain fields represent an average over the imaging duration rather than an instantaneous snapshot. This temporal smoothing could underestimate fast or transient events.

At the cell periphery, the strain values extracted from DVC represent averages over subvolumes encompassing both membrane and adjacent cytoplasm. Consequently, the reaction forces reconstructed from FEM represent smoothed mechanical responses rather than forces strictly localized at the membrane. This averaging should be considered when interpreting biological relevance, as it may lead to overestimation or spatial blurring of localized forces. The reaction forces obtained in this study range from 0 to 40 pN over a 6 min interval. In the literature, variable values are reported. For example, 2D TFM measurements of murine 3T3 cells show a maximum force of 120 nN over a few minutes (Dembo and Wang, 1999), while the human colorectal cancer cell line SW 480 exhibits a reaction force up to 10 nN over 10 h (Makarchuk et al., 2018). However, using the integrative tension sensor (ITS) method, different magnitudes are observed, including a maximum force of 54 pN exerted by platelets within 4 min (Wang et al., 2018). It is important to note that the stresses and forces exerted by the cell on its environment depend on several factors, including the measurement time interval, cell adhesion, and substrate stiffness. Cellular forces and stresses are concentrated at the cell-substrate interface. By examining the position of the reaction forces, we observe that the cell propels itself by exerting a greater force in the opposite direction to its overall movement, using the substrate. Cells use a system of punctual adhesions and invadopodia at the cell-substrate interface to move through space. This movement is achieved through actin filament polymerization, actomyosin contraction, and other proteins regulating this process (Schwarz and Soiné, 2015; Svitkina, 2018).

Different kinematics, stress and force fields were observed for three cells placed in the same environment, highlighting the multifactorial complexity of their behaviour. To extend the results, particularly for understanding invadopodia formation, it would be useful to investigate a larger sample of cells, use substrates of different stiffness and embed the cell in the substrate to represent the diversity of ECM mechanics in vivo. We have explored a direct method of modelling the problem, using measured displacement fields to compute stress and force fields. Subsequently, solving the inverse problem could increase the accuracy of the simulations and provide a more detailed understanding of the mechanical mechanisms underlying cellular behaviour such as cell invasion.

In the present model, the cell was treated as a homogeneous, isotropic, linearly elastic material with a single Young's modulus of 0.5 kPa, consistent with reported average values (Pogoda et al., 2014). This assumption was necessary for computational tractability but neglects the spatial heterogeneity of subcellular structures such as nucleus, cytoskeleton, and membrane (Lu et al., 2006). As a result, the reconstructed stress distributions should be interpreted as averaged representations. Future developments of this approach should incorporate region-specific or viscoelastic material properties to enhance biological fidelity. The present simplified representation significantly reduces model complexity and computational cost, facilitating the analysis of

multiple time points. Thus, our current stress and force estimations likely represent an oversimplification of the actual mechanical states inside the cell.

It should be noted that strains measured at the cell periphery using DVC represent averages over finite subvolumes that include both the plasma membrane and adjacent cytoplasm. While this implies that reconstructed reaction forces reflect an averaged response rather than strictly membrane-level forces, it also constitutes a distinctive feature of the present approach. Unlike methods restricted to probing the substrate (e.g. TFM) or to localized point indentations (e.g. AFM), our methodology provides a volumetric, full-field quantification that inherently integrates submembrane and intracellular mechanics. This makes it a complementary extension of prior AFM and nanomechanics works (Shen et al., 2020; Bahwini et al., 2018; Bahwini et al., 2022; Khataee et al., 2013; Khataee et al., 2018), but applied at the whole-cell level in invasive cancer cells.

Future improvements of this method should prioritize experimental validation via TFM and integration of more realistic viscoelastic and heterogeneous mechanical models, thus significantly enhancing physiological relevance and predictive accuracy.

5. Conclusions

Cell kinetics is a complex process influenced by various intracellular and microenvironmental factors. Cellular biomechanics can provide insights into the mechanisms of cell migration and invasion, particularly in pathologies such as cancer. In this study, a novel method has been developed for the quantification and visualization of mechanical full fields within cells by integrating confocal microscopy, Digital Volume Correlation (DVC), and Finite Element Method (FEM). This method was applied to cancer cells, revealing internal displacement and stress fields during cellular development over time. Understanding these dynamics can help elucidate the interaction of biological parameters and facilitate new in silico therapeutic approaches by targeting cell behaviour.

This study establishes a foundational methodology for intracellular mechanical characterization through integrated imaging, correlation, and simulation approaches. Future developments will include direct mechanical validation (e.g., TFM), improved mechanical modeling (heterogeneous and viscoelastic), and extension of the method to 3D cell cultures, thus enhancing the method's robustness and physiological relevance.

CRediT authorship contribution statement

Aurélie Gangneux: Writing - original draft, Visualization, Validation, Software, Methodology, Investigation, Formal analysis, Data curation, Conceptualization. Aymerick Gaboriau: Writing - original draft, Visualization, Methodology, Formal analysis, Data curation. Laetitia Caille: Writing - original draft, Validation, Supervision, Methodology, Formal analysis, Conceptualization. Marc Mesnil: Writing - original draft, Supervision, Project administration, Investigation, Formal analysis, Conceptualization. Prasanth Bokam: Writing original draft, Software, Resources, Project administration, Formal analysis. Tanguy Vendeuvre: Writing - original draft, Supervision, Resources, Project administration, Formal analysis, Conceptualization. Stéphane Sebille: Writing – original draft, Supervision, Methodology, Formal analysis, Conceptualization. Norah Defamie: Writing - original draft, Validation, Supervision, Project administration, Methodology, Formal analysis, Data curation, Conceptualization. Arnaud Germaneau: Writing - original draft, Validation, Supervision, Project administration, Methodology, Formal analysis, Conceptualization.

Declaration of competing interest

The authors declare that they have no known competing financial interests or personal relationships that could have appeared to influence

the work reported in this paper.

Acknowledgements

The authors would like to thank the platform Interactifs LabEx (ANR-11-LABX-0017-01), Ansys, the Platform ImageUP and Ligue contre le Cancer for supporting this work.

Data availability

Data will be made available on request.

References

- Apolinar-Fernández, A., Barrasa-Fano, J., Cóndor, M., Van Oosterwyck, H., Sanz-Herrera, J.A., 2023. Traction force reconstruction assessment on real three-dimensional matrices and cellular morphologies. Int. J. Eng. Sci. 186, 103828. https://doi.org/10.1016/j.ijengsci.2023.103828.
- Bahwini, T., Zhong, Y., Gu, C., Choi, K.-S., 2022. System identification of biological cells by atomic force microscopy. Int. J. Interact. Des. Manuf. 16, 691–702. https://doi. org/10.1007/s12008-022-00861-w.
- Bahwini, T.M., Zhong, Y., Gu, C., Nasa, Z., Oetomo, D., 2018. Investigating the mechanical properties of biological brain cells with atomic force microscopy. J. Med. Dev. Trans. ASME 12, 041007
- Butler, J.P., Tolić-Nørrelykke, I.M., Fabry, B., Fredberg, J.J., 2002. Traction fields, moments, and strain energy that cells exert on their surroundings. Am. J. Physiol.-Cell Physiol. 282, C595–C605. https://doi.org/10.1152/ajpcell.00270.2001.
- Chenouard, N., Smal, I., De Chaumont, F., Maška, M., Sbalzarini, I.F., Gong, Y., Cardinale, J., Carthel, C., Coraluppi, S., Winter, M., Cohen, A.R., Godinez, W.J., Rohr, K., Kalaidzidis, Y., Liang, L., Duncan, J., Shen, H., Xu, Y., Magnusson, K.E.G., Jaldén, J., Blau, H.M., Paul-Gilloteaux, P., Roudot, P., Kervrann, C., Waharte, F., Tinevez, J.-Y., Shorte, S.L., Willemse, J., Celler, K., Van Wezel, G.P., Dan, H.-W., Tsai, Y.-S., De Solórzano, C.O., Olivo-Marin, J.-C., Meijering, E., 2014. Objective comparison of particle tracking methods. Nat. Methods 11, 281–289. https://doi.org/10.1038/nmeth.2808.
- Cheung, B.C., Chen, X., Davis, H.J., Nordmann, C.S., Toth, J., Hodgson, L., Segall, J.E., Shenoy, V.B., Wu, M., 2025. Identification of CD44 as a key engager to hyaluronic acid-rich extracellular matrices for cell traction force generation and tumor invasion in 3D. Matrix Biol. 135, 1–11.
- Chepied, A., Daoud-Omar, Z., Meunier-Balandre, A.C., Laird, D.W., Mesnil, M., Defamie, N., 2020. Involvement of the gap junction protein, Connexin43, in the formation and function of invadopodia in the human U251 glioblastoma cell line. Cells 9 (1), 117. https://doi.org/10.3390/cells9010117, 2020 Jan 3.
- Dembo, M., Harris, A.K., 1981. Motion of particles adhering to the leading lamella of crawling cells. J. Cell Biol. 91, 528–536. https://doi.org/10.1083/jcb.91.2.528.
- Dembo, M., Wang, Y.-L., 1999. Stresses at the cell-to-substrate interface during locomotion of fibroblasts. Biophys. J. 76, 2307–2316. https://doi.org/10.1016/ S0006-3495(99)77386-8.
- Doyle, A.D., Nazari, S.S., Yamada, K.M., 2022. Cell-extracellular matrix dynamics. Phys. Biol. 19, 021002. https://doi.org/10.1088/1478-3975/ac4390.
- Emami, N., Sedaei, Z., Ferdousi, R., 2021. Computerized cell tracking: current methods, tools and challenges. Vis. Inform. 5, 1–13. https://doi.org/10.1016/j. visinf.2020.11.003.
- Franck, C., Maskarinec, S.A., Tirrell, D.A., Ravichandran, G., 2011. Three-Dimensional traction force microscopy: a new tool for quantifying cell-matrix interactions. PLoS One 6, 1–15. https://doi.org/10.1371/journal.pone.0017833.
- Franck, C., Hong, S., Maskarinec, S.A., Tirrell, D.A., Ravichandran, G., 2007. Three-dimensional full-field measurements of large deformations in soft materials using confocal microscopy and digital volume correlation. Exp. Mech. 47, 427–438. https://doi.org/10.1007/s11340-007-9037-9.
- Germaneau, A., Doumalin, P., Dupré, J.C., 2007. Full 3D measurement of strain field by scattered light for analysis of structures. Exp. Mech. 47, 523–532. https://doi.org/ 10.1007/s11340-006-9029-1.
- Holenstein, C.N., Lendi, C.R., Wili, N., Snedeker, J.G., 2019. Simulation and evaluation of 3D traction force microscopy. Comput. Methods Biomech. Biomed. Eng. 22, 853–860. https://doi.org/10.1080/10255842.2019.1599866.
- Hur, S.S., Zhao, Y., Li, Y.-S., Botvinick, E., Chien, S., 2009. Live cells exert 3-dimensional traction forces on their substrata. Cell. Mol. Bioeng. 2, 425–436. https://doi.org/ 10.1007/s12195-009-0082-6.
- Khataee, H., Naseri, S., Zhong, Y., Liew, A.W., 2018. Unbinding of kinesin from microtubule in the strongly bound states enhances under assisting forces. Mol. Informatics 37, 1700092. https://doi.org/10.1002/minf.201700092.
- Khataee, H.R., Liew, A.W.C., Zhong, Y., Hanifehpour, Y., Joo, S.W., 2013.
 A computational study of physical properties of the smallest fullerene, C20 nanoparticle. J. Comput. Theor. Nanosci. 10, 1908–1913.
- Kornilov, A., Safonov, I., 2018. An overview of watershed algorithm implementations in open source libraries. J. Imaging 4, 123. https://doi.org/10.3390/jimaging4100123.
- Legant, W.R., Miller, J.S., Blakely, B.L., Cohen, D.M., Genin, G.M., Chen, C.S., 2010.
 Measurement of mechanical tractions exerted by cells in three-dimensional matrices.
 Nat. Methods 7, 969–971. https://doi.org/10.1038/nmeth.1531.

- Lekka, M., Gnanachandran, K., Kubiak, A., Zieliński, T., Zemła, J., 2021. Traction force microscopy – measuring the forces exerted by cells. Micron 150, 103138. https:// doi.org/10.1016/j.micron.2021.103138.
- Louis, D.N., Perry, A., Wesseling, P., Brat, D.J., Cree, I.A., Figarella-Branger, D., Hawkins, C., Ng, H.K., Pfister, S.M., Reifenberger, G., Soffietti, R., von Deimling, A., Ellison, D.W., 2021. The 2021 WHO classification of tumors of the central nervous system: a summary. Neuro Oncol. 23 (8), 1231–1251. https://doi.org/10.1093/neuonc/noab106, 2021 Aug 2.
- Lu, Y.B., Franze, K., Seifert, G., Steinhäuser, C., Kirchhoff, F., Wolburg, H., et al., 2006. Viscoelastic properties of individual glial cells and neurons in the CNS. Proc. Natl. Acad. Sci. USA 103 (47), 17759–17764. https://doi.org/10.1073/pnas.0606150103.
- Makarchuk, S., Beyer, N., Gaiddon, C., Grange, W., Hébraud, P., 2018. Holographic traction force microscopy. Sci. Rep. 8, 3038. https://doi.org/10.1038/s41598-018-21206-2.
- Masi, I., Caprara, V., Bagnato, A., Rosanò, L., 2020. Tumor cellular and microenvironmental Cues controlling invadopodia formation. Front. Cell Dev. Biol. 8, 584181. https://doi.org/10.3389/fcell.2020.584181, 2020 Oct 15.
- Manzo, C., Garcia-Parajo, M.F., 2015. A review of progress in single particle tracking: from methods to biophysical insights. Rep. Prog. Phys. 78, 124601. https://doi.org/ 10.1088/0034-4885/78/12/124601.
- Meijering, E., Dzyubachyk, O., Smal, I., 2012. Methods for cell and particle tracking. In: Methods in Enzymology. Elsevier, pp. 183–200. https://doi.org/10.1016/B978-0-12-391857-4.00009-4.
- Monzo, P., Crestani, M., Chong, Y.K., Ghisleni, A., Hennig, K., Li, Q., Kakogiannos, N., Giannotta, M., Richichi, C., Dini, T., 2021. Adaptive mechanoproperties mediated by the formin FMN1 characterize glioblastoma fitness for invasion. Dev. Cell 56, 2841–2855
- Mulligan, J.A., Bordeleau, F., Reinhart-King, C.A., Adie, S.G., 2018. Traction force microscopy for noninvasive imaging of cell forces. In: Dong, C., Zahir, N., Konstantopoulos, K. (Eds.), Biomechanics in Oncology, Advances in Experimental Medicine and Biology. Springer International Publishing, Cham, pp. 319–349. https://doi.org/10.1007/978-3-319-95294-9_15.
- Ou, A., Yung, W.K.A., Majd, N., 2020. Molecular mechanisms of treatment resistance in glioblastoma. Int. J. Mol. Sci. 22 (1), 351. https://doi.org/10.3390/ijms22010351, 2020 Dec 31.
- Parekh, A., Ruppender, N.S., Branch, K.M., Sewell-Loftin, M.K., Lin, J., Boyer, P.D., Candiello, J.E., Merryman, W.D., Guelcher, S.A., Weaver, A.M., 2011. Sensing and modulation of invadopodia across a wide range of rigidities. Biophys. J. 100, 573–582. https://doi.org/10.1016/j.bpj.2010.12.3733.
- Peschetola, V., Laurent, V.M., Duperray, A., Michel, R., Ambrosi, D., Preziosi, L., Verdier, C., 2013. Time-dependent traction force microscopy for cancer cells as a measure of invasiveness. Cytoskeleton 70, 201–214. https://doi.org/10.1002/ cm.21100.
- Pogoda, K., Chin, L., Georges, P.C., Byfield, F.J., Bucki, R., Kim, R., Weaver, M., Wells, R. G., Marcinkiewicz, C., Janmey, P.A., 2014. Compression stiffening of brain and its effect on mechanosensing by glioma cells. New J. Phys. 16, 075002. https://doi.org/10.1088/1367-2630/16/7/075002.
- Pushkarsky, I., Liu, Y., Weaver, W., Su, T.-W., Mudanyali, O., Ozcan, A., Di Carlo, D., 2014. Automated single-cell motility analysis on a chip using lensfree microscopy. Sci. Rep. 4, 4717. https://doi.org/10.1038/srep04717.
- Qian, H., Sheetz, M.P., Elson, E.L., 1991. Single particle tracking. Analysis of diffusion and flow in two-dimensional systems. Biophys. J. 60, 910–921. https://doi.org/10.1016/S0006-3495(91)82125-7.
- Rico, F., Roca-Cusachs, P., Gavara, N., Farré, R., Navajas, D., 2005. Probing mechanical properties of living cells by atomic force microscopy with blunted pyramidal cantilever tips. Phys. Rev. 72 (2). https://doi.org/10.1103/PhysRevE.72.021914.
- Sabass, B., Gardel, M.L., Waterman, C.M., Schwarz, U.S., 2008. High resolution traction force microscopy based on experimental and computational advances. Biophys. J. 94, 207–220. https://doi.org/10.1529/biophysj.107.113670.
- Sanz-Herrera, J.A., Barrasa-Fano, J., Cóndor, M., Van Oosterwyck, H., 2021. Inverse method based on 3D nonlinear physically constrained minimisation in the framework of traction force microscopy. Soft Matter 17, 10210–10222. https://doi. org/10.1039/DOSM00789G.
- Saxton, M.J., Jacobson, K., 1997. SINGLE-PARTICLE TRACKING:applications to membrane dynamics. Annu. Rev. Biophys. Biomol. Struct. 26, 373–399. https://doi. org/10.1146/annurev.biophys.26.1.373.
- Schwarz, U.S., Soiné, J.R.D., 2015. Traction force microscopy on soft elastic substrates: a guide to recent computational advances. Biochim. Biophys. Acta BBA - Mol. Cell Res. 1853, 3095–3104. https://doi.org/10.1016/j.bbamcr.2015.05.028.
- Sergé, A., Bertaux, N., Rigneault, H., Marguet, D., 2008. Dynamic multiple-target tracing to probe spatiotemporal cartography of cell membranes. Nat. Methods 5, 687–694. https://doi.org/10.1038/nmeth.1233.
- Shen, T., Shirinzadeh, B., Zhong, Y., Smith, J., Pinskier, J., Ghafarian, M., 2020. Sensing and modelling mechanical response in large deformation indentation of adherent cell using atomic force microscopy. Sensors 20 (6). https://doi.org/10.3390/ s20061764
- Song, D., Hugenberg, N., Oberai, A.A., 2019. Three-dimensional traction microscopy with a fiber-based constitutive model. Comput. Meth. Appl. Mech. Eng. 357, 112579. https://doi.org/10.1016/j.cma.2019.112579.
- Svitkina, T., 2018. The actin cytoskeleton and actin-based motility. Cold Spring Harbor Perspect. Biol. 10, a018267. https://doi.org/10.1101/cshperspect.a018267.
- Toyjanova, J., Bar-Kochba, E., López-Fagundo, C., Reichner, J., Hoffman-Kim, D., Franck, C., 2014. High resolution, large deformation 3D traction force microscopy. PLoS One 9, e90976. https://doi.org/10.1371/journal.pone.0090976.

- Trepat, X., Wasserman, M.R., Angelini, T.E., Millet, E., Weitz, D.A., Butler, J.P., Fredberg, J.J., 2009. Physical forces during collective cell migration. Nat. Phys. 5, 426–430. https://doi.org/10.1038/nphys1269.
- Valle, V., Bokam, P., Germaneau, A., Hedan, S., 2019. New development of digital volume correlation for the study of fractured materials. Exp. Mech. 59, 1–15. https://doi.org/10.1007/s11340-018-0415-2.
- Wang, Y., LeVine, D.N., Gannon, M., Zhao, Y., Sarkar, A., Hoch, B., Wang, X., 2018.
 Force-activatable biosensor enables single platelet force mapping directly by fluorescence imaging. Biosens. Bioelectron. 100, 192–200. https://doi.org/10.1016/i.bios.2017.09.007.
- Wang, Z., Wang, X., Zhang, Y., Xu, W., Han, X., 2021. Principles and applications of single particle tracking in cell research. Small 17, 2005133. https://doi.org/ 10.1002/smll.202005133.
- Weihs, D., Mason, T.G., Teitell, M.A., 2006. Bio-microrheology: a frontier in microrheology. Biophys. J. 91, 4296–4305. https://doi.org/10.1529/ biophysj.106.081109.
- Wolf, K., Wu, Y.I., Liu, Y., Geiger, J., Tam, E., Overall, C., Stack, M.S., Friedl, P., 2007. Multi-step pericellular proteolysis controls the transition from individual to collective cancer cell invasion. Nat. Cell Biol. 9, 893–904. https://doi.org/10.1038/ ncb1616.
- Yang, Z., Lin, J.-S., Chen, J., Wang, J.H.-C., 2006. Determining substrate displacement and cell traction fields—a new approach. J. Theor. Biol. 242, 607–616. https://doi. org/10.1016/j.jtbi.2006.05.005.